## How chain dynamics affects crack initiation in double-network gels

Yong Zheng<sup>a,b</sup>, Takahiro Matsuda<sup>c</sup>, Tasuku Nakajima<sup>b,c,1</sup>, Wei Cui<sup>c</sup>, Ye Zhang<sup>a</sup>, Chung-Yuen Hui<sup>d</sup>, Takayuki Kurokawa<sup>c</sup>؈, and Jian Ping Gong<sup>b,c,1</sup>؈

aGraduate School of Life Science, Hokkaido University, Sapporo 001-0021, Japan; bInstitute for Chemical Reaction Design and Discovery, Hokkaido University, Sapporo 001-0021, Japan; cFaculty of Advanced Life Science, Hokkaido University, Sapporo 001-0021, Japan; and dField of Theoretical and Applied Mechanics, Sibley School of Mechanical and Aerospace Engineering, Cornell University, Ithaca, NY 14853

Edited by Zhigang Suo, Harvard University, Cambridge, MA, and approved October 29, 2021 (received for review June 28, 2021)

Double-network gels are a class of tough soft materials comprising two elastic networks with contrasting structures. The formation of a large internal damage zone ahead of the crack tip by the rupturing of the brittle network accounts for the large crack resistance of the materials. Understanding what determines the damage zone is the central question of the fracture mechanics of doublenetwork gels. In this work, we found that at the onset of crack propagation, the size of necking zone, in which the brittle network breaks into fragments and the stretchable network is highly stretched, distinctly decreases with the increase of the solvent viscosity, resulting in a reduction in the fracture toughness of the material. This is in sharp contrast to the tensile behavior of the material that does not change with the solvent viscosity. This result suggests that the dynamics of stretchable network strands, triggered by the rupture of the brittle network, plays a role. To account for this solvent viscosity effect on the crack initiation, a delayed blunting mechanism regarding the polymer dynamics effect is proposed. The discovery on the role of the polymer dynamic adds an important missing piece to the fracture mechanism of this unique material.

chain dynamics  $\mid$  crack initiation  $\mid$  double-network gels  $\mid$ nonlinear crack tip analysis

n recent decades, many tough soft materials have been developed (1–6), greatly expanding the application range of soft materials in various fields, such as artificial cartilages (7, 8), soft robotics (9-11), and stretchable electronics (12-15). Understanding the fracture mechanisms of these materials is critical for their applications, but it poses fundamental challenges considering the strongly nonlinear elasticity and dissipative deformation involved.

Generally, crack initiation and growth in soft materials involve a wide range of time and length scales, including molecular-scale covalent bond scission (4, 16-20), nanoscale polymer network dynamics, mesoscale energy dissipation (4, 21-23), and macroscale crack blunting (18, 19, 24). The integration of various approaches from chemistry, polymer physics, and continuum mechanics are required to reveal the full picture of the fracture process. To date, most research on soft material fracture has focused on the meso- and macroscale. At these relatively large scales, the continuum mechanics theory is applicable, and the deformation surrounding the crack tip can be directly observed experimentally. According to nonlinear elastic fracture mechanics theories, two basic length scales, the nonlinear elastic length scale (or elasto-adhesive length),  $\ell$ , and the dissipative length scale,  $\xi$ , are relevant to the fracture initiation of highly deformable soft materials (18, 19, 25). The  $\ell$  represents the typical distance from a crack tip below which the deformation is dominated by strongly nonlinear elasticity (18). The length scale  $\xi$  represents the size of the region surrounding the crack tip where the stress or strain concentration is eliminated, and it scales with the size of the dissipation zone (18, 26, 27). These two length scales  $\ell$  and  $\xi$  are related to the fracture

energy  $\Gamma$ , the elastic modulus E, and the work of extension to fracture  $W^*$ , as  $\ell \sim \Gamma/E$  and  $\xi \sim \Gamma/W^*$ . For tough soft materials,  $\ell$  and  $\xi$  are typically in a 10- $\mu$ m to 10-cm range, and  $\ell > \xi$ because the work of extension to fracture is usually greater than the elastic modulus  $(W^* > E)$  for these materials (18). Yet what determines these length scales and how they are related to the specific structure of the materials are hardly known. To answer these questions, studies at the polymer network scale is indispensable. Because the molecular failure processes strongly depend on the polymer network architecture and molecular interactions, the fracture mechanism at this length scale shows individuality and richness.

Double-network (DN) gels, a class of tough soft materials composed of two interpenetrated elastic networks with contrasting structures, are a relatively simple system to address these questions due to their rate-independent deformation behavior and negligible molecular interactions. The role of polymer dynamics on fracture of DN gels is the focus of this work. The contrasting network structure of DN gels is formed by a two-step sequential polymerization process. The first network, densely cross-linked, is stiff and brittle; the second network, sparsely cross-linked, is soft and stretchable. DN gels show fracture energy  $\Gamma$  orders of magnitude larger than either of the individual components (28). The remarkable toughness enhancement of DN gels originates from the sacrificial rupture of the brittle network over a wide zone (damage zone) around

## **Significance**

Fracture in soft materials often couples a wide range of time and length scales. To date, research is mostly focused at the meso- and macroscale in which the continuum mechanics approach is expected to work, and the deformation surrounding the crack tip can be directly observed. Yet understanding at the network scale is very limited. A relevant question is how does chain dynamics at the network scale control fracture in rate-independent materials? Here, we study the role of polymer dynamics on the fracture and nonlinear crack tip behaviors of rate-independent double-network gels. We believe this work is crucially important for understanding the dynamic molecular process of fracture and for further facilitating theoretical approaches to predict failure in soft materials.

Author contributions: Yong Zheng, T.M., T.N., and J.P.G. designed research; Yong Zheng performed research; Yong Zheng, T.M., T.N., W.C., Ye Zhang, C.-Y.H., T.K., and J.P.G. analyzed data; and Yong Zheng, T.N., and J.P.G. wrote the paper.

The authors declare no competing interest.

This article is a PNAS Direct Submission.

Published under the PNAS license.

<sup>1</sup>To whom correspondence may be addressed. Email: tasuku@sci.hokudai.ac.jp or gong@sci.hokudai.ac.jp.

This article contains supporting information online at http://www.pnas.org/lookup/ suppl/doi:10.1073/pnas.2111880118/-/DCSupplemental.

Published November 30, 2021.

the crack tip, while the stretchable network maintains the structural integrity of the combined networks (29). Such a mechanism suppresses the stress concentration and dissipates a large amount of mechanical energy at the crack tip. The covalent bond rupture near the crack tip has been confirmed chemically using luminescent probes or mechano-radical polymerization (3, 30). Because the DN effect is essentially based on the network topological architecture rather than specific molecular interactions, it has been applied to a wide range of polymer combinations, including gels and solvent-free elastomers (3, 31–34).

The deformation of unnotched DN gels is rate independent at a conventional strain rate (usually less than  $10^1~\rm s^{-1}$ ) because the dynamics of network strands is much faster than the deformation rate (28, 35–38). Furthermore, in tearing tests, DN gels have a very weak tearing velocity dependence in the fracture energy and damage zone size (37–39). Weak stress relaxation, on the other hand, was observed, suggesting a time-dependent effect in DN gels (40). Our question is the following: Does the chain dynamics at the network scale influence the fracture of the rate-independent materials? In theory, one expects that the rupture of the brittle network triggers the load transfer of the stretchable network, and hence, its dynamics might influence the stress redistribution and extension of internal fracture, thereby the nonlinear, energy dissipative behavior at the crack tip.

The dynamics of the polymer network in a solvated gel is governed by the hydrodynamic friction between the monomeric unit and the solvent, as described by the Rouse-like motion (41–43). In this work, we tune the polymer network dynamics of DN gels by varying the solvent viscosity  $\eta_s$ . Ethylene glycol (EG)/water mixtures and glycerol/water mixtures are used to study the effect of viscosity. These mixture solvents have a comparable solvent quality to water with regard to the constitutive

polymers of DN gels, as confirmed by almost the same swelling ratios, and the tensile behaviors of unnotched DN gels. This allows us to investigate the effect of polymer network dynamics by varying solvent viscosity over a range  $10^0$  to  $10^3$  times of water. We observed that the fracture energy measured by a pure-shear test of notched specimens decreases significantly with increasing solvent viscosity. This decrease in fracture toughness is directly related to the reduction of the necking zone size around the crack tip as solvent viscosity increases. We present an explanation on the finding in terms of the dynamics of the stretchable network in transferring the load during the formation of the damage zone.

## **Results and Discussion**

Our experiments were conducted with DN gels comprising poly(2-acrylamido-2-methylpropane sulfonic acid sodium salt) (PNaAMPS) as the first network and polyacrylamide (PAAm) as the second network, both of which were synthesized in water via a two-step polymerization process (29). The synthesized PNaAMPS/PAAm DN hydrogels were swollen in water to achieve equilibrium and then immersed in EG/water or glycerol/water mixtures to achieve swelling equilibrium in the new solvents. The DN gels swollen in EG/water mixtures and glycerol/water mixtures are labeled as  $\mathrm{DN_{EG^-}}\phi$  and  $\mathrm{DN_{glycerol^-}}\phi$ , respectively, in which  $\phi$  is the volume fraction of the organic solvent.

We start with  $\mathrm{DN_{EG^-}}\phi$ . As  $\phi$  increases from 0 to 1.0, the viscosity of the EG/water mixtures increases by a factor of 20 from 0.89 mPa·s for water to 17.12 mPa·s for EG at 25 °C (*SI Appendix*). The swelling ratios of the DN gels and the corresponding single-network (SN) gels are all weakly dependent on  $\phi_{\mathrm{EG}}$ , indicating that EG and the EG/water mixtures have the

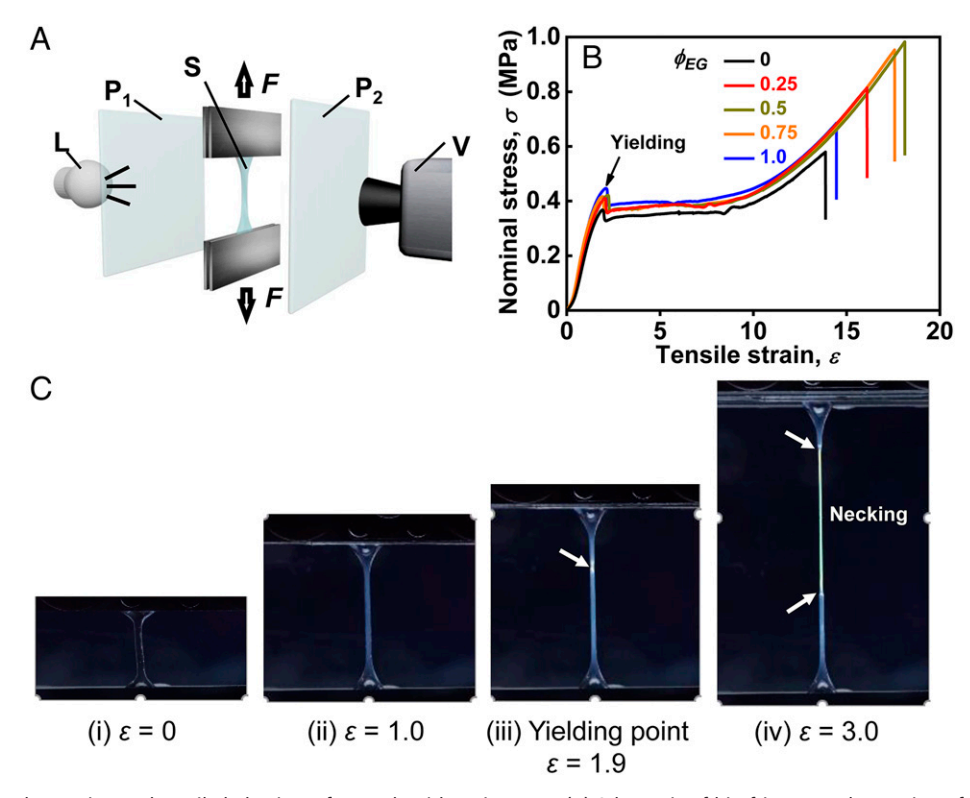


Fig. 1. Birefringence observation and tensile behaviors of DN gels with various  $\phi_{EG}$ . (A) Schematic of birefringence observation of tensile process for DN gels. L: lamp; P<sub>1</sub>, P<sub>2</sub>: crossed circular polarized films; S: sample; and V: video camera. (B) Nominal stress σ-tensile strain ε curves of DN gels swelled in EG/ water mixture with  $\phi_{EG}$  varied from 0 (pure water) to 1.0 (pure EG). (C) Birefringence images of DN<sub>EG</sub>-0 gel under uniaxial stretching at various tensile strains:  $\varepsilon = 0$  (i);  $\varepsilon = 1.0$  (ii); yielding point  $\varepsilon = 1.9$  (iii); and  $\varepsilon = 3.0$  (iv). The necking zone (shown by arrows) appears above the yielding point, showing strong white birefringence.

same solvent quality as water for both networks and DN gels (*SI Appendix*, Fig. S1). Hence, the DN structure in these solvents could be considered as the same, and we can study the effect of solvent viscosity on the crack initiation of DN gels.

Uniaxial tensile tests were performed prior to the fracture tests. The nominal strain rate was 0.14 s<sup>-1</sup>. The experimental setup shown in Fig. 1A was used to perform real-time imaging of birefringence during the tensile process (24). The birefringence reveals the degree of network strand orientation during deformation (44). The sample was placed between two crossed circular polarized films, and the two films were placed between a white lamp and a video camera. The birefringence during tensile process was recorded with the video camera (24 frames/s,  $1,920 \times 1,080$  pixels). Fig. 1B shows that the tensile behaviors of DN gels are hardly influenced by the change of solvents as revealed by the well overlapped tensile stress-strain curves for different solvents. The small difference between the curves in Fig. 1B is due to the slight volume change using the different solvents (SI Appendix, Fig. S2B). The rupture points varied significantly, even for the same solvent (SI Appendix, Fig. S2 A and E), implying that the rupture of these unnotched DN gels is governed by preexisting defects of the DN structure. The tensile behavior of the DN gels was rate independent (SI Appendix, Fig. S3). The DN gels exhibited remarkable stress yielding, which corresponds to the onset of necking in the samples (Fig. 1C and SI Appendix, Fig. S4). As the strain increases, the necking zone expands, while the unnecking region regresses. In the necking region, the brittle network is considered to rupture into fragments, and the second network strands are highly stretched (28, 36). The necking region exhibits strong birefringence because the network strands are highly stretched and oriented along the tensile direction (Fig. 1C and SI Appendix, Fig. S4).

We then performed the pure shear fracture tests on prenotched DN specimens with a geometry shown in Fig. 24. The

nominal global deformation rate was 0.06 s<sup>-1</sup>. To identify the necking zone around the crack tip, we performed real-time imaging of the birefringence of the sample. Despite nearly identical tensile curves for the unnotched samples (Fig. 1B), pure-shear fracture tests revealed that the crack initiation resistance of the DN gels strongly depend on the solvent. Fig. 2B presents the nominal stress-stretch ratio curves for the prenotched DN specimens with various  $\phi_{\rm EG}$  from loading to the onset of crack growth. Although all the curves overlap before crack growth, the critical stretch ratio  $\lambda_c$  and stress  $\sigma_c$  at which the crack begins to grow are significantly reduced as  $\phi_{\mathrm{EG}}$ increases. As shown in Fig. 2C, the threshold  $\lambda_c$  decreases with increasing  $\phi_{\rm EG}$ . Specifically, as  $\phi_{\rm EG}$  increases,  $\lambda_{\rm c}$  decreases gradually from 2.07 ( $\phi_{\rm EG}=0$ ) to 1.58 ( $\phi_{\rm EG}=1.0$ ). This decreasing  $\lambda_c$  results in reduced toughness with increasing  $\phi_{EG}$ . Fig. 2D depicts the dependence of fracture energy  $\Gamma$  on  $\phi_{\rm EG}$ .  $\Gamma$ is estimated from the area under the stress-strain curves of the corresponding unnotched specimens to  $\lambda_c$  and the initial specimen height  $H_0$  (SI Appendix, Fig. S5) following the literature (45). DN gels, in particular, show a significant reduction in fracture energy  $\Gamma$  from 3,000 J·m<sup>-2</sup> for  $\phi_{\rm EG} = 0$  to 700 J·m<sup>-2</sup> for  $\phi_{\rm EG} = 1.0$ .

The real-time imaging of the birefringence allows us to directly study crack blunting and yielding around the crack tip of the DN gels. As typical examples, images of crack shape profile for DN<sub>EG</sub>-0, DN<sub>EG</sub>-0.5, and DN<sub>EG</sub>-1.0 samples at the onset of crack propagation are shown in Fig. 3A, and we extracted the crack shape for different  $\phi_{EG}$  in Fig. 3B. The DN<sub>EG</sub>-0 shows significant crack blunting. With increasing  $\phi_{EG}$ , the crack tip profile gradually becomes less blunted, and the magnitude of the crack tip opening decreases. The critical crack tip opening displacement (CTOD, or  $2\delta_c$ ), defined as the crack opening spanned by two symmetric rays originating from the crack tip with a 90° angle between them (18) at fracture, provides a condition for the initiation of crack growth. Fig. 3C depicts  $\phi_{EG}$ 

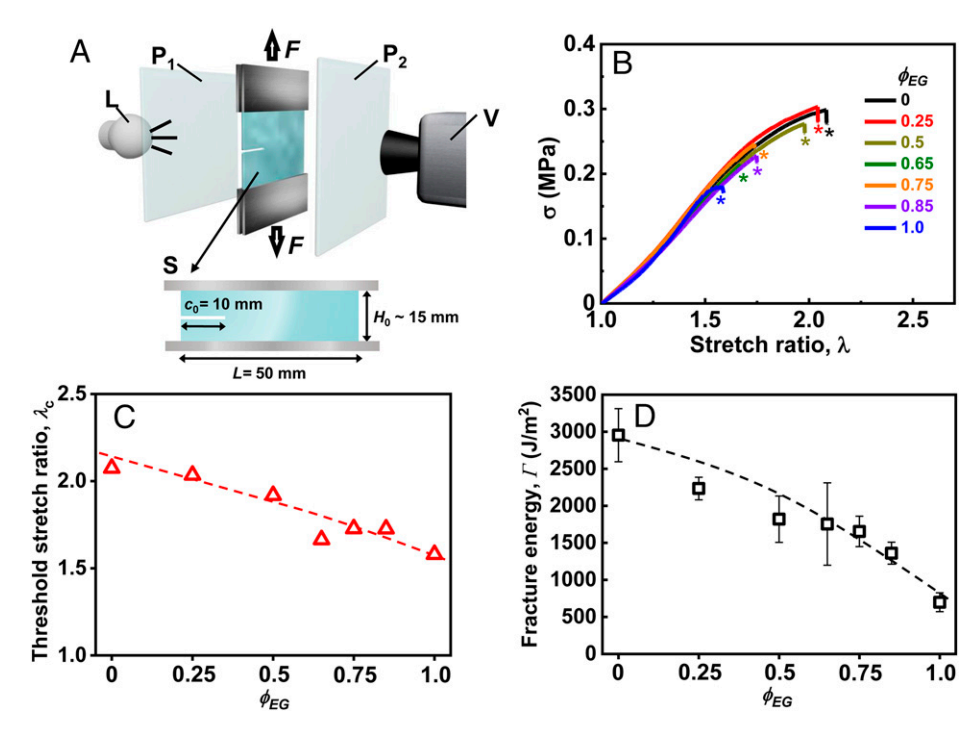


Fig. 2. Birefringence observation and pure shear fracture behaviors of DN gels with various  $\phi_{EG}$ . (A) Schematic of real-time birefringence observation of fracture process for DN gels in pure shear test. L: lamp; P<sub>1</sub>, P<sub>2</sub>: crossed circular polarized films; S: sample; and V: video camera. (B) Nominal stress σ-stretch ratio  $\lambda$  curves of notched DN gels with various  $\phi_{EG}$  in the pure-shear fracture test before crack growth. The asterisks indicate the onset of crack growth. (C) Dependence of the critical stretch ratio  $\lambda_c$  at the onset of crack growth on  $\phi_{EG}$ . The data points correspond to B. (D) Fracture energy Γ obtained from pure-shear fracture tests as a function of  $\phi_{EG}$ . The data points are the average values with SD of three measurements for each sample.

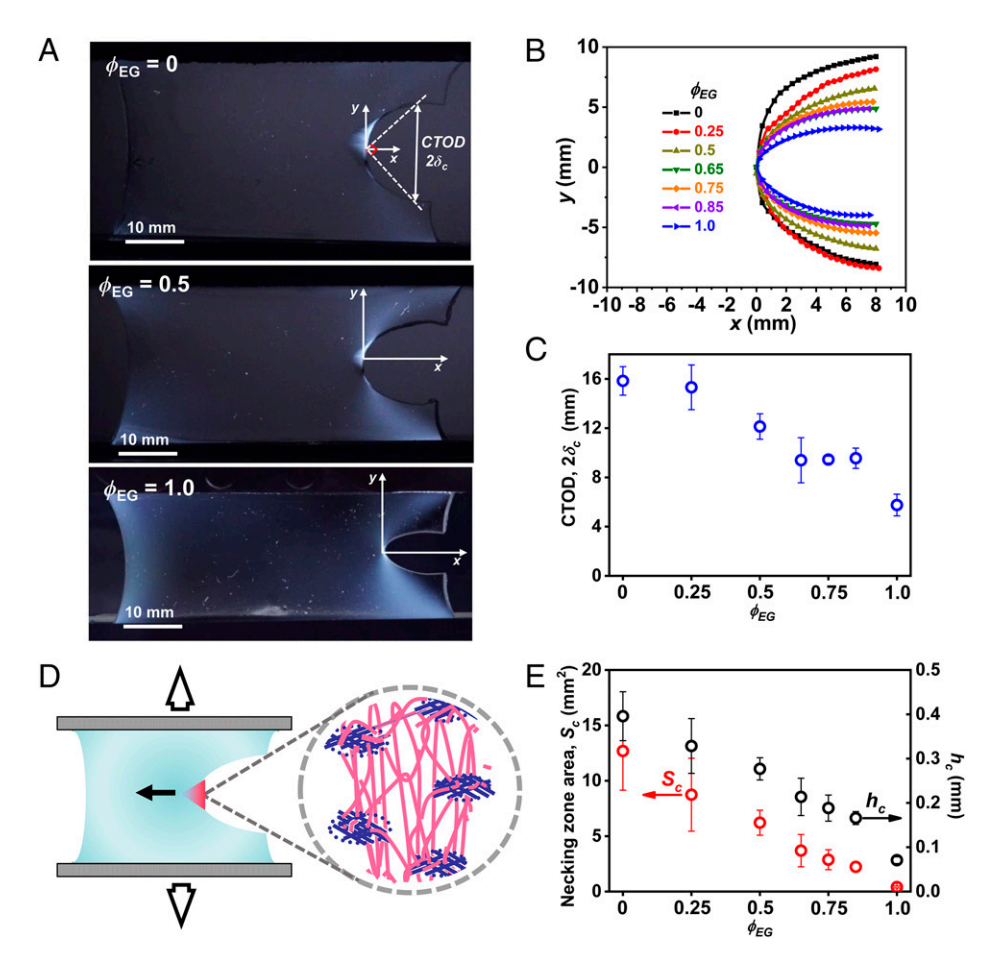


Fig. 3. Birefringence images and crack tip behaviors of DN gels with various  $\phi_{EG}$  at the onset of crack growth. (A) Birefringence images around the crack tip for  $\phi_{EG} = 0$ , 0.5, and 1.0. (B) Crack tip profiles of DN gels with various  $\phi_{EG}$ . (C) Critical CTOD,  $2\delta_c$  defined in A as a function of  $\phi_{EG}$ . (D) Schematic illustration of network structure in the necking zone ahead of the crack tip as seen by strong birefringence area in A. (E) Average necking zone area  $S_c$  in deformed state and necking zone size  $h_c$  at undeformed state as functions of  $\phi_{EG}$  (average of three parallel tests).

dependence of  $2\delta_c$ . Notably, the  $2\delta_c$  gradually decreases from 16 mm for the DN<sub>EG</sub>-0 gel to 6 mm for the DN<sub>EG</sub>-1.0 gel, indicating a reduction in crack blunting ability prior to crack growth.

In the DN<sub>EG</sub>-0 gels, a large bright birefringence area was observed in front of the crack tip as shown in Fig. 3A. This bright area represents the necking zone around the crack tip as illustrated in Fig. 3D and as seen in the tensile tests (Fig. 1C and SI Appendix, Fig. S4). The birefringence area decreases with increasing  $\phi_{\rm EG}$  and becomes so small that it could hardly be observed in DN<sub>EG</sub>-1.0 gel. The critical necking zone area  $S_c$ (mm<sup>2</sup>) at the deformed state is estimated from the strong birefringence area ahead of crack tips for different  $\phi_{EG}$  as shown in Fig. 3E. The  $S_c$  in the deformed state of the gels decreases monotonically with increasing  $\phi_{\rm EG}$ . The characteristic necking zone size at the undeformed state,  $h_c$ , was roughly estimated from the square root of  $S_c$  using the relation  $h_c = S_c^{0.5}/\lambda_n$ , in which  $\lambda_n$  is the stretch ratio of the necking region. Here, we assumed that the stretch ratio of every material point in the necking zone at the crack tip is the same as the material point in the strong birefringence necking region in the uniaxial tension test. We used this uniaxial approximation because previous studies showed that for a highly deformable soft solid under mode I plane stress conditions, uniaxial tension dominates the stress field near the crack tip (18, 25).  $\lambda_n = 9.0$  was estimated from the stretching ratio in the necking region in the uniaxial tensile test (SI Appendix, Fig. S6) and was found independent of  $\phi_{\rm EG}$ . As shown in Fig. 3E,  $h_c$  decreases with increasing  $\phi_{\rm EG}$ , and the size of the necking zone  $h_c$  observed in this work for DN gels in water ( $\phi_{\rm EG}=0$ ) is consistent with previous studies (38, 46). In previous studies, the damage zone thickness h was determined using optical microscopes and may have included unnecked regions where the first network rupture occurs by random bond scission. Regardless of the difference in method, the necking zone  $h_c$  observed in this study is of the same order of magnitude as h in these previous studies.

To confirm if the observed phenomenon is generic, we further performed the same measurement of DN gels in glycerol/water mixtures, which have a much wider range of viscosity (SI Appendix, Fig. S7A). Glycerol/water mixtures also have similar solvent quality as water to the DN gels (SI Appendix, Fig. S7B). The experiments were performed using a different batch of DN gels that had similar tensile behavior to that of EG/water mixtures (SI Appendix, Fig. S8). In glycerol/water mixtures, the fracture energy, necking zone, and crack blunting also obviously decrease as glycerol fraction  $\phi_{\rm glycerol}$  increases, similar to the behavior in EG/water mixtures (SI Appendix, Fig. S7 C–E).

For both two series of samples with EG/water mixture and glycerol/water mixture as solvents, we observed that the fracture energy  $\Gamma$  linearly correlates to the necking zone size  $h_c$  with a proportional constant of 6.5 MJ/m³ (Fig. 4.4). This result clearly shows that increasing the solvent viscosity suppresses the ability of the DN gels to form a large necking zone ahead of the crack tip, which accounts for the reduced fracture toughness.

Next, we use the nonlinear elastic fracture mechanics theory to quantitatively explain the linear correlation between  $\Gamma$  and

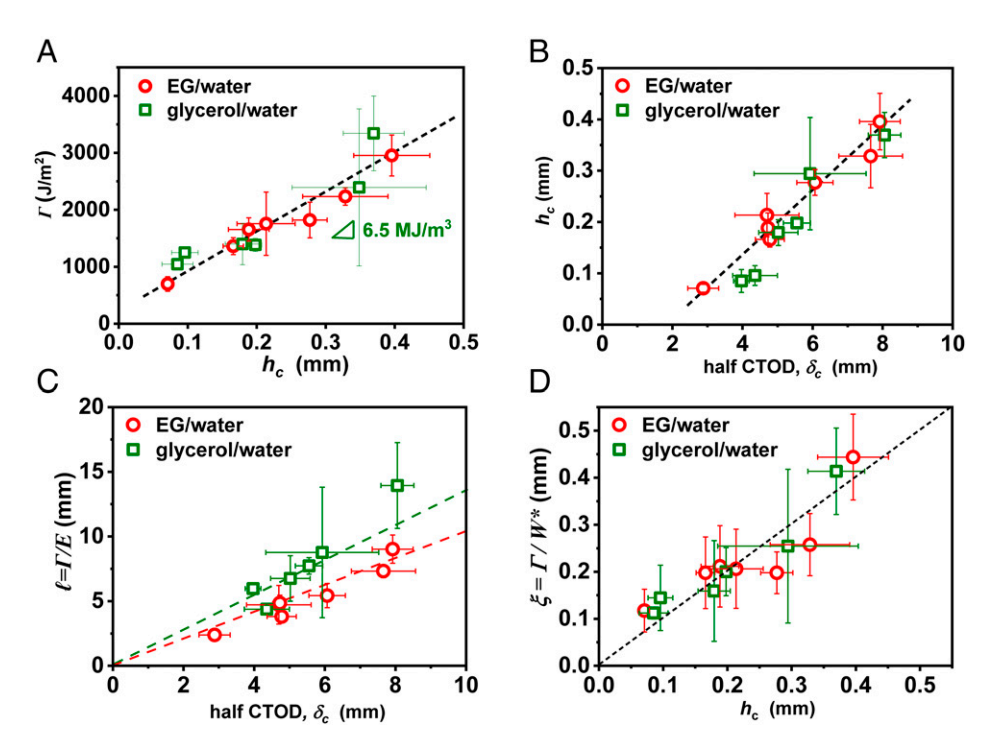


Fig. 4. Strong coupling of multiscale length scales of nonlinear elastic crack tip of DN gels. (A) Correlation between fracture energy  $\Gamma$  and necking zone size  $h_c$ . (B) Correlation between  $h_c$  and the half CTOD  $\delta_c$ . (C) Correlation between nonlinear, elastic length  $\ell$  and  $\delta_c$ . (D) Correlation between the dissipative length  $\xi$  and  $h_c$ .  $\ell$  and  $\xi$  were estimated from the nonlinear, elastic fracture theory.

 $h_c$ . For crack tip fields in generalized neo-Hookean soft elastic solids subjected to large deformation in mode I, the asymptotic near-tip stress field is dominated by tension and has the form  $\sigma_T = \alpha \frac{T}{r}$ , in which  $\sigma_T$  is the true stress in tension direction, r is the radial coordinate of a material point in the undeformed configuration, and  $\alpha$  is a numerical constant that depends on the angular coordinate and strain hardening characteristics (18, 25). By setting the asymptotic near-tip stress field (true stress,  $\sigma_T$ ) to the true critical stress for necking (yielding),  $\sigma_{T, \nu}$ , and r to the necking zone size  $h_c$ , we obtain  $\sigma_{T,y} = \alpha \frac{\Gamma}{h_c}$ . Because  $\sigma_{T,y}$ and  $\alpha$  are all independent of solvents,  $\Gamma$  and  $h_c^{n_c}$  should be proportional to each other. We estimated the numerical constant  $\alpha$  $\sim 0.2$  from the slope of the linear regression (6.5 MJ/m<sup>3</sup>) in Fig. 4A and the true yielding stress  $\sigma_{T,y} \sim 1.2$  to 1.7 MPa, which is the product of the nominal critical yielding stress and stretch ratio in the tensile test (SI Appendix, Table S1). In theory, the constant  $\alpha$  is exactly  $1/\pi \sim 0.32$  for a neo-Hookean solid (18, 25). Our experimental observations yielded comparable results. The quantitative consistency of the  $\Gamma$ - $h_c$  relationship with the necking stress confirms that increasing  $\phi_{EG}$  or  $\phi_{glycerol}$  reduces the toughness of the DN gels, which is directly related to necking zone reduction near the crack tip.

We also discovered that the macroscale crack blunting correlates well with the size of the mesoscale necking zone. As shown in Fig. 4B, the half CTOD  $\delta_c$  is linearly correlated with the necking zone size  $h_c$  with a slope of 0.06. This linear relationship between  $\delta_c$  and  $h_c$  clearly indicates that the macroscale blunting is intrinsically determined by the formation of the mesoscale necking zone.

The rate-independent deformation of the DN gels allows us to use the nonlinear elastic fracture mechanics theory to discuss the macro- and mesoscale behaviors. For various generalized neo-Hookean incompressible materials, the theory predicts that the half CTOD ( $\delta_c$ ) takes the form  $\delta_c \sim (\Gamma/E)^{\beta} \sim \ell^{\beta}$ , in which  $\beta$  varies  $\sim$ 0.8 to 1.1 (18, 25). As a result of the scaling analysis, the relation  $\delta_c \sim \ell$  should be approximately valid for a wide range of highly deformable soft materials (18, 25). To

examine the validity of this scaling for the DN gels, we plot the nonlinear elastic length scale  $\ell = \Gamma/E$  versus  $\delta_c$  for various  $\phi_{\rm EG}$  and  $\phi_{\rm glycerol}$  in Fig. 4C. We used the elastic modulus E estimated from the pure shear specimens in this case. We observe a good linear correlation of  $\ell \sim \delta_c$  for two series of samples with mixture solvents, which agrees well with the theoretical prediction of nonlinear elastic fracture mechanics.

To examine whether the necking zone size at undeformed state  $h_c$  is correlated to the dissipative length scale  $\xi$ , we calculated  $\xi \sim \Gamma/W^*$ , in which  $W^*$  is the critical energy per unit volume for material failure.  $W^*$  was determined from the work of extension to fracture of the unnotched samples in uniaxial tensile deformation (the area under the stress–strain curves in Fig.1B and SI Appendix, Table S1). As shown in Fig. 4D,  $h_c$  and  $\xi$  are nearly equal; that is,  $h_c \approx \xi$ . This finding indicates that the crack tip load transfer length for the DN gels is nearly identical to the average necking zone size. The length scale  $\xi$  is commonly defined as the size of the region surrounding the crack tip, where the stress or strain concentration because of the crack is eliminated by dissipative processes (18). The result of  $h_c \approx \xi$  is reasonable because significant dissipation occurs in the necking region due to chain breakage.

Finally, we discuss the molecular mechanism to determine necking zone size  $h_c$ . In Fig. 5, we show that the two sets of results in EG/water mixtures and glycerol/water mixtures well overlap on a plot of  $h_c$  versus the solvent viscosity  $\eta_s$ . In a small viscosity regime (solvent viscosity range of 0.89 to 20 mPa·s),  $h_c$  roughly follows a power law relation  $h_c \sim \eta_s^{-0.5}$ , whereas in a large viscosity regime,  $h_c$  becomes constant. Notably, the saturation of  $h_c$  at high viscosity is not due to the spatial limitation of the measurement, considering we observed a linear correlation between  $h_c$  and the fracture energy  $\Gamma$  for all viscosity ranges (Fig. 4A). This result clearly indicates that the network dynamics controls necking zone size at the onset of crack propagation. To clarify if the global deformation rate also influences the necking zone formation around the crack tip, we further performed the birefringence imaging of crack tips for DN gels

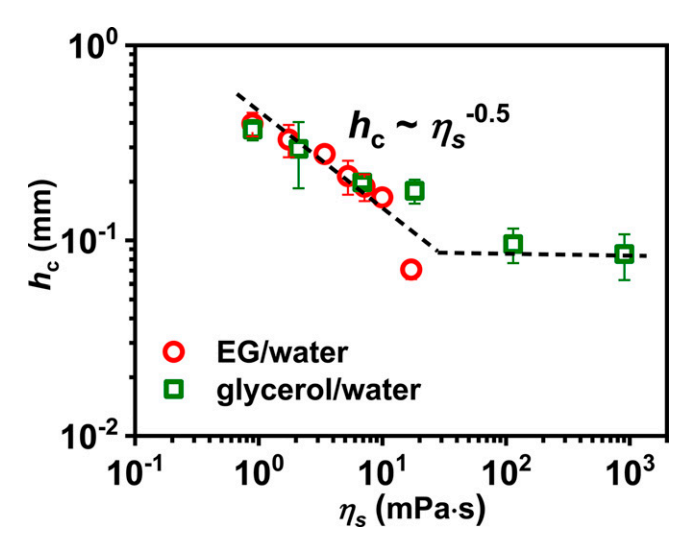


**Fig. 5.** Relation between necking zone size  $h_c$  and solvent viscosity  $\eta_s$ . Log-log plot of necking zone size  $h_c$  and viscosity of solvent  $\eta_s$  for two series of samples with EG/water mixture and glycerol/water mixture as solvents.  $h_c$  roughly follows a power law relation of  $h_c \sim \eta_s^{-0.5}$  at a low-viscosity regime and becomes constant at a large viscosity regime. The dashed line is a guide for eyes.

with various  $\phi_{\rm EG}$  subjected to different loading velocities. The necking zone size at the onset of crack propagation hardly changes with loading velocity over three orders of magnitude from 0.5 to 1,000 mm/min, corresponding to a global strain rate range of  $5.6\times10^{-4}$  to  $1.1~{\rm s}^{-1}$  for DN gels with different  $\phi_{\rm EG}$  (SI Appendix, Figs. S9–S11). These findings are reasonable because the strain rate at the crack tip, although being amplified to some extent in comparison to the global strain rate, is still slow enough when compared to the dynamics of polymer strands, and the two networks behave elastically before rupture. Specifically, the Rouse-like dynamics of PAAm hydrogels have been observed at time scales faster than  $10^{-3}$  to  $10^{-5}$  s (47). This time scale is much shorter than the inverse of the deformation rate in the tensile test and pure shear test of this study.

Therefore, the viscosity effect on necking zone size should be related to the Rouse-like dynamic process that is much faster than the applied loading rate.

How does the fast polymer network dynamics influence the necking zone size around the crack tip  $h_c$ ? We hypothesize that the dynamics of the second network governs the local deformation rate at the time of the first network rupture, which influences the local stress redistribution and necking zone development. First, we consider the expansion of necking zone and the crack opening with the increase of global stretch  $\lambda$  (Fig. 6). Upon stretching, stress is concentrated around the crack tip, which leads to the rupture of the first network there. Once the first network strand ruptures, the load carried by this first network is immediately transferred to the second network, causing the second network to extend. Then, strain hardening of the second network induces further rupture of the neighboring brittle network, thereby expanding the necking zone and resulting in blunting (increase of crack tip opening displacement  $2\delta$ ). The necking zone expanding and crack blunting suppress the stress concentration at the crack tip and prevent crack propagation. This process is repeated, and the necking zone size h increases with increase in stretching  $\lambda$  until the tensile stress at the crack tip, where the stress is most concentrated, reaches a level sufficient to activate the bond scission of the second network strands that bridge the crack. When the critical value,  $\lambda_c$ , is exceeded, the crack with a necking zone size  $h_c$  begins to advance. Here, we consider the effect of second network dynamics on the necking zone increment from h to  $h + \Delta h$ . By a quasistatic global stretch increment  $\Delta \lambda$ , the stress also increases quasistatically until the breaking of the brittle network in the necking front region from h to  $h + \Delta h$ , and the stress in this region is immediately transferred to the second network. However, because of the Rouse-like relaxation of the second network strands, it takes a time,  $\tau_R$ , for the second network strands in  $\Delta h$  to extend; therefore, the stress redistribution and the crack tip opening is delayed by a time of  $\tau_R$ . As a result, a transient stress overshoot appears in the region h immediately after an increment of  $\Delta\lambda$ and decays to a lower level after  $\tau_R$ . That is, when  $\lambda$  is increased to  $\lambda + \Delta \lambda$ , the necking zone advances from h to  $h + \Delta h$ , and the crack tip opening displacement increases from  $2\delta$  to  $2(\delta + \Delta\delta)$ with a time lag governed by the second network relaxation of

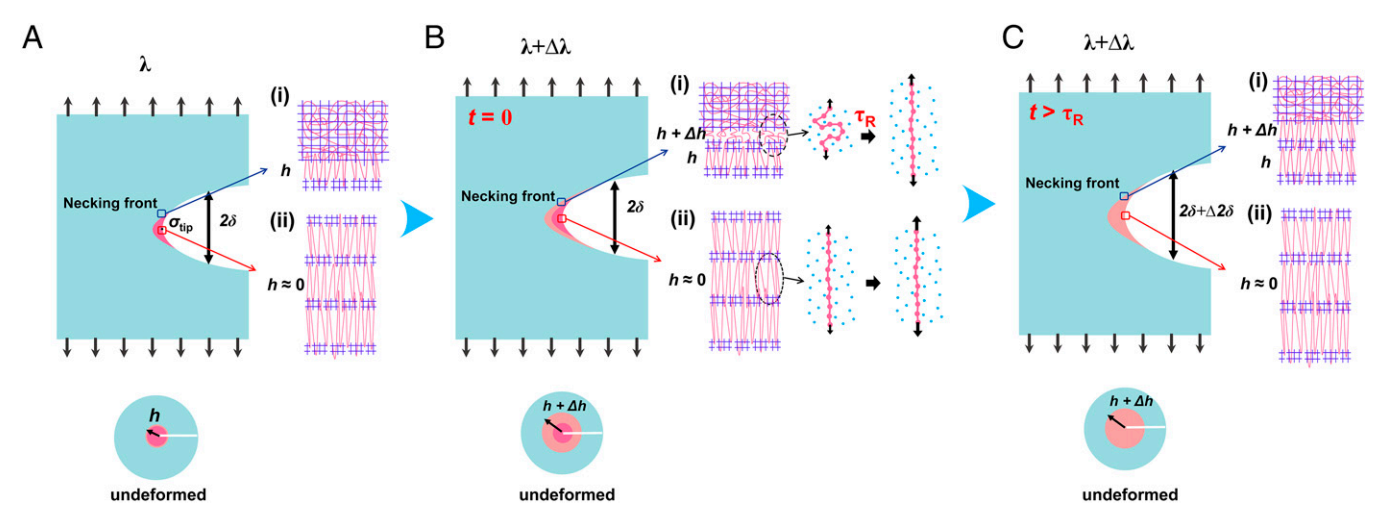


Fig. 6. Possible explanation for the dynamic effect of second network on the critical necking zone size  $h_c$  for crack initiation. (A) A global stretch  $\lambda$  results in a necking zone size h and crack tip opening displacement  $2\delta$ . (B) An increment  $\Delta\lambda$  causes further breaking of the brittle network in the necking front region  $\Delta h$ , and the stress in this region is immediately transferred to the second network. However, it takes a time,  $\tau_R$ , for the second network strands to be stretched into extended conformation in the newly formed necking zone. (C) As a result, the crack blunting to  $2(\delta + \Delta\delta)$  is delayed by a time  $\tau_R$ . Such a time lag results in a stress overshoot around the crack. When the stress is large enough to activate the bond breaking of the second network at the crack tip, the crack propagates. Because the Rouse-like relaxation time  $\tau_R$  is proportional to the solvent viscosity, in a high-viscosity solvent, the probability to induce bond breaking is high, and the necking zone size  $h_c$  at crack initiation decreases. See text for detailed explanation.

wnloaded at Cornell University Library on February 7, 202

 $\tau_R$ . Because  $\tau_R$  is much shorter than the inverse of the global stretch rate, such dynamic effect does not appear in the tensile test (Fig. 1B) and crack opening process (SI Appendix, Fig. S12) before the onset of crack propagation (the stress at crack tip is well below the threshold of the second network). It does, however, have an effect on the critical stretch ratio  $\lambda_c$  for crack propagation, which is the point that the stress overshoot at the crack tip is large enough to activate the bond scission of the second network (SI Appendix, Fig. S13). Because the Rouse time is proportional to the solvent viscosity (41), the stress on the crack tip decays slowly at high viscosity, increasing the likelihood of bond scission at the same  $\lambda$ . As a result, the crack advances at a lower  $\lambda_c$ , with a smaller necking zone size  $h_c$  for a more viscous solvent. According to polymer physics (41), the stress relaxation modulus as a function of time, t, of polymers is given by  $G(t) \sim$  $(\tau_R/t)^{1/2}$  within the Rouse time. Because  $\tau_R$  is proportional to  $\eta_s$  (41), the short-time modulus G(t) of the second network at a time scale shorter than  $\tau_R$  should scale with the solvent viscosity  $\eta_s$  as  $G(t) \sim \eta_s^{0.5}$ . The observed relation between the necking zone size and solvent viscosity,  $h_c \sim \eta_s^{-0.5}$ , is probably related to this short-time modulus dependence on the viscosity.

It should be noted that the above discussion only considers the solvent viscosity effect on the polymer dynamics, ignoring the possible contribution from inter- or intramolecular interactions between polymer strands at an increased fraction of highly viscous solvents. In the presence of these interchain interactions, the resistance to strand rearrangement of the second network upon deformation may be greater than the pure friction from solvent viscosity. Even when these possible molecular interactions are considered, the picture of chain dynamics effect still holds.

This study demonstrates that, despite DN gels being made up of two elastic networks, the dynamics of the second network, which is much faster than the global deformation rate, has a

- J. P. Gong, Y. Katsuyama, T. Kurokawa, Y. Osada, Double-network hydrogels with extremely high mechanical strength. Adv. Mater. 15, 1155–1158 (2003).
- 2. J.-Y. Sun et al., Highly stretchable and tough hydrogels. Nature 489, 133–136 (2012).
- 3. E. Ducrot, Y. Chen, M. Bulters, R. P. Sijbesma, C. Creton, Toughening elastomers with sacrificial bonds and watching them break. *Science* **344**, 186–189 (2014).
- 4. C. Creton, 50th anniversary perspective: Networks and gels: Soft but dynamic and tough. *Macromolecules* **50**, 8297–8316 (2017).
- E. Filippidi et al., Toughening elastomers using mussel-inspired iron-catechol complexes. Science 358, 502–505 (2017).
- T. L. Sun et al., Physical hydrogels composed of polyampholytes demonstrate high toughness and viscoelasticity. Nat. Mater. 12, 932–937 (2013).
- 7. A. S. Hoffman, Hydrogels for biomedical applications. *Adv. Drug Deliv. Rev.* **64**, 18–23 (2012).
- 8. M. A. Haque, T. Kurokawa, J. P. Gong, Super tough double network hydrogels and their application as biomaterials. *Polymer (Guildf.)* **53**, 1805–1822 (2012).
- H. Yuk et al., Hydraulic hydrogel actuators and robots optically and sonically camouflaged in water. Nat. Commun. 8, 14230 (2017).
- P. Polygerinos et al., Soft robotics: Review of fluid-driven intrinsically soft devices; manufacturing, sensing, control, and applications in human-robot interaction. Adv. Eng. Mater. 19, 1700016 (2017).
- M. Cianchetti, C. Laschi, A. Menciassi, P. Dario, Biomedical applications of soft robotics. Nat. Rev. Mater. 3, 143–153 (2018).
- C. Keplinger et al., Stretchable, transparent, ionic conductors. Science 341, 984–987 (2013).
- J. A. Rogers, T. Someya, Y. Huang, Materials and mechanics for stretchable electronics. Science 327, 1603–1607 (2010).
- 14. C. Yang, Z. Suo, Hydrogel ionotronics. Nat. Rev. Mater. 3, 125–142 (2018).
- S. Lin et al., Stretchable hydrogel electronics and devices. Adv. Mater. 28, 4497–4505 (2016).
- G. Lake, A. Thomas, The strength of highly elastic materials. Proc. R. Soc. Lond. A Math. Phys. Sci. 300, 108–119 (1967).
- 17. R. Bai, J. Yang, Z. Suo, Fatigue of hydrogels. *Eur. J. Mech. A, Solids* **74**, 337–370 (2019).
- R. Long, C.-Y. Hui, J. P. Gong, E. Bouchbinder, The fracture of highly deformable soft materials: A tale of two length scales. Annu. Rev. Condens. Matter Phys. 12, 71–94 (2021).
- C. Creton, M. Ciccotti, Fracture and adhesion of soft materials: A review. Rep. Prog. Phys. 79 (046601 (2016)
- T. Sakai, Y. Akagi, S. Kondo, U. Chung, Experimental verification of fracture mechanism for polymer gels with controlled network structure. Soft Matter 10, 6658–6665 (2014).

strong influence on the critical stretching ratio  $\lambda_c$  and necking zone size for crack propagation. The second network relaxation delays the crack blunting and causes stress overshoot around the crack tip, which increases the probability to activate the bond breakage of the second network and results in a smaller damage zone at the onset of crack propagation. This knowledge, we believe, is crucially important for understanding the dynamic molecular process of fracture and for further theoretical analysis to predict fractures in soft materials.

## **Materials and Methods**

**Materials.** 2-Acrylamido-2-methylpropanesulfonic acid sodium salt (Toagosei Co., Ltd.), acrylamide (Junsei Chemical Co. Ltd.), N,N-methylenebis(acrylamide) (Wako Pure Chemical Industries, Ltd.), α-ketoglutaric acid (Wako Pure Chemical Industries, Ltd.), and glycerol (Wako Pure Chemical Industries, Ltd.), and glycerol (Wako Pure Chemical Industries, Ltd.) were used as received. Milli-Q water (resistivity: 18.3  $M\Omega$ /cm) was used in all experiments.

**Synthesis of DN Gels.** The PNaAMPS/PAAm DN hydrogels were synthesized by a two-step sequential network formation technique following the literature (29).

All details associated with sample preparations, solvent viscosity calculation, procedures of reswelling samples in EG/water mixture and glycerol/water mixture, tensile tests, pure-shear fracture tests and real-time birefringence observation, and an estimation of stretch ratio in necking region are available in *SI Appendix*.

Data Availability. All study data are included in the article and/or SI Appendix.

ACKNOWLEDGMENTS. This research is supported by the Japan Society for the Promotion of Science (JSPS) KAKENHI (Grant Nos. JP17H06144, JP17H04891, and JP19K23617) and by Japan Science and Technology Agency (JST), Precursory Research for Embryonic Science and Technology (PRESTO) Grant No. JPMJPR2098. C.-Y.H. is supported by the NSF under Grant No. CMMI-1903308. Yong Zheng thanks the China Scholarship Council for financial support during his PhD studies.

- T. Zhang, S. Lin, H. Yuk, X. Zhao, Predicting fracture energies and crack-tip fields of soft tough materials. Extreme Mech. Lett. 4, 1–8 (2015).
- H. R. Brown, A model of the fracture of double network gels. Macromolecules 40, 3815–3818 (2007).
- Y. Tanaka, A local damage model for anomalous high toughness of double-network gels. EPL 78, 56005 (2007).
- F. Luo et al., Crack blunting and advancing behaviors of tough and self-healing polyampholyte hydrogel. Macromolecules 47, 6037–6046 (2014).
- R. Long, C.-Y. Hui, Crack tip fields in soft elastic solids subjected to large quasi-static deformation—A review. Extreme Mech. Lett. 4, 131–155 (2015).
- C. Chen, Z. Wang, Z. Suo, Flaw sensitivity of highly stretchable materials. Extreme Mech. Lett. 10, 50–57 (2017).
- Y. Wang, X. Yang, G. Nian, Z. Suo, Strength and toughness of adhesion of soft materials measured in lap shear. J. Mech. Phys. Solids 143, 103988 (2020).
- 28. J. P. Gong, Why are double network hydrogels so tough? *Soft Matter* **6**, 2583–2590
- S. Ahmed, T. Nakajima, T. Kurokawa, M. A. Haque, J. P. Gong, Brittle–ductile transition of double network hydrogels: Mechanical balance of two networks as the key factor. *Polymer (Guildf.)* 55. 914–923 (2014).
- T. Matsuda, R. Kawakami, T. Nakajima, J. P. Gong, Crack tip field of a doublenetwork gel: Visualization of covalent bond scission through mechanoradical polymerization. *Macromolecules* 53, 8787–8795 (2020).
- T. Nakajima et al., A universal molecular stent method to toughen any hydrogels based on double network concept. Adv. Funct. Mater. 22, 4426–4432 (2012).
- 32. T. Nakajima et al., Tough double-network gels and elastomers from the nonprestretched first network. ACS Macro Lett. 8, 1407–1412 (2019).
- T. Matsuda, T. Nakajima, J. P. Gong, Fabrication of tough and stretchable hybrid double-network elastomers using ionic dissociation of polyelectrolyte in nonaqueous media. *Chem. Mater.* 31, 3766–3776 (2019).
- P. Millereau et al., Mechanics of elastomeric molecular composites. Proc. Natl. Acad. Sci. U.S.A. 115, 9110–9115 (2018).
- T. Matsuda et al., Yielding criteria of double network hydrogels. Macromolecules 49, 1865–1872 (2016).
- T. Nakajima, T. Kurokawa, S. Ahmed, W.-I. Wu, J. P. Gong, Characterization of internal fracture process of double network hydrogels under uniaxial elongation. Soft Matter 9, 1955–1966 (2013).
- 37. Y. Tanaka et al., Determination of fracture energy of high strength double network hydrogels. J. Phys. Chem. B 109, 11559–11562 (2005).

Downloaded at Cornell University Library on February 7, 2022

- Q. M. Yu, Y. Tanaka, H. Furukawa, T. Kurokawa, J. P. Gong, Direct observation of damage zone around crack tips in double-network gels. *Macromolecules* 42, 3852–3855 (2009).
- 39. H. Furukawa *et al.*, Tear velocity dependence of high-strength double network gels in comparison with fast and slow relaxation modes observed by scanning microscopic light scattering. *Macromolecules* **41**, 7173–7178 (2008).
- 40. I. Kolvin, J. M. Kolinski, J. P. Gong, J. Fineberg, How supertough gels break. *Phys. Rev. Lett.* 121. 135501 (2018).
- 41. M. Rubinstein, R. H. Colby, *Polymer Physics* (Oxford University Press, New York, 2003)
- 42. H. Takahashi, Y. Ishimuro, H. Watanabe, Viscoelastic behavior of scarcely crosslinked poly (dimethyl siloxane) gel. *Nihon Reoroji Gakkaishi* **34**, 135–145
- 43. H. Takahashi, Y. Ishimuro, H. Watanabe, Viscoelastic behavior of scarcely crosslinked poly (dimethyl siloxane) gels: 2. Effects of sol component and network strand length. *Nihon Reoroji Gakkaishi* 35, 191–198 (2007).
- 44. K. Fukao *et al.*, Effect of relative strength of two networks on the internal fracture process of double network hydrogels as revealed by in situ small-angle X-ray scattering. *Macromolecules* **53**, 1154–1163 (2020).
- 45. R. Long, C.-Y. Hui, Fracture toughness of hydrogels: Measurement and interpretation. *Soft Matter* **12**, 8069–8086 (2016).
- S. Liang et al., Direct observation on the surface fracture of ultrathin film doublenetwork hydrogels. Macromolecules 44, 3016–3020 (2011).
- B. A. Krajina et al., Dynamic light scattering microrheology reveals multiscale viscoelasticity of polymer gels and precious biological materials. ACS Cent. Sci. 3, 1294–1303 (2017).